

1 Detection of breast cancer lymph node metastases in frozen sections with a point-of-
2 care low-cost microscope scanner

3 Oscar Holmström^{1*}, Nina Linder^{1,2}, Hannu Moilanen³, Antti Suutala¹, Stig Nordling⁴,
4 Anders Ståhls⁵, Mikael Lundin¹, Vinod Diwan⁶, Johan Lundin^{1,6}

5

6 ¹Institute for Molecular Medicine Finland (FIMM), University of Helsinki, Helsinki,
7 Finland

8 ²Department of Women's and Children's Health, International Maternal and Child
9 health, Uppsala University, Uppsala, Sweden

10 ³Center of Microscopy and Nanotechnology, University of Oulu, Finland

11 ⁴Department of Pathology, University of Helsinki, Helsinki, Finland

12 ⁵Helsinki University Hospital and HUSLAB Pathology laboratory, Helsinki, Finland

13 ⁶Department of Public Health Sciences, Karolinska Institutet, Stockholm, Sweden

14

15 *Corresponding author: oscar.holmstrom@helsinki.fi (OH)

16

17 Email addresses of authors: O. Holmström: oscar.holmstrom@helsinki.fi, N. Linder:

18 nina.linder@helsinki.fi, A. Ståhls: anders.stahls@hus.fi, S. Nordling:

19 stig.nordling@helsinki.fi, M. Lundin: mikael.lundin@helsinki.fi, H. Moilanen:

20 hannu.moilanen@ee.oulu.fi, A. Suutala: antti.suutala@helsinki.fi, V. Diwan:

21 vinod.diwan@ki.se, J. Lundin: johan.lundin@helsinki.fi

22 **Abstract**

23 **Background** Detection of lymph node metastases is essential in breast cancer
24 diagnostics and staging, affecting treatment and prognosis. Intraoperative
25 microscopy analysis of sentinel lymph node frozen sections is standard for detection
26 of axillary metastases, but requires access to a pathologist for sample analysis.
27 Remote analysis of digitized samples is an alternative solution, but is limited by the
28 requirement for high-end slide scanning equipment. **Objective** To determine whether
29 the image quality achievable with a low-cost, miniature digital microscope scanner is
30 sufficient for detection of metastases in breast cancer lymph node frozen sections.
31 **Methods** Lymph node frozen sections from 79 breast cancer patients were digitized
32 using a prototype miniature microscope scanner and a high-end slide scanner.
33 Images were independently reviewed by two pathologists and results compared
34 between devices with conventional light microscopy analysis as ground truth.
35 **Results** Detection of metastases in the images acquired with the miniature scanner
36 yielded an overall sensitivity of 91 % and specificity of 99 % and showed strong
37 agreement when compared to light microscopy ($k = 0.91$). Strong agreement was
38 also observed when results were compared to results from the high-end slide
39 scanner ($k = 0.94$). A majority of discrepant cases were micrometastases and
40 sections of which no anticytokeratin staining was available. **Conclusion** Accuracy of
41 detection of metastatic cells in breast cancer sentinel lymph node frozen sections by
42 visual analysis of samples digitized using low-cost, point-of-care microscopy is
43 comparable to analysis of digital samples scanned using a high-end, whole slide
44 scanner. This technique could potentially provide a workflow for digital diagnostics in
45 resource-limited settings, facilitate sample analysis at the point-of-care and reduce
46 the need for trained experts on-site during surgical procedures.

47 **Introduction**

48 Breast cancer is the most common form of cancer in women, and the second leading
49 cause of cancer-related death in women globally [1]. Detection of axillary lymph node
50 metastases remains essential for the staging of breast cancer, affecting treatment
51 and prognosis [2]. Presence of axillary lymph node metastases indicates a need for
52 more extensive surgical procedures, typically axillary lymph node dissection (ALND)
53 [3]. Axillary metastases can be detected accurately using sentinel lymph node
54 biopsies in the vast majority of node positive patients, thus avoiding unnecessary
55 further axillary surgery for node negative patients [4, 5]. This is important as
56 evacuation of axillary lymph nodes is a major cause of postoperative complications
57 [6]. Intraoperative evaluation of frozen sections from sentinel lymph nodes (FS) is
58 the most common technique to determine axillary lymph node status, but requires
59 the presence of a pathologist on-site or close to the point-of-care to analyze the
60 samples. Surgical pathology using FS is generally considered accurate for the
61 detection of macrometastases, but not as reliable for detection of smaller lesions, i.e.
62 micrometastases and isolated tumor cells [7, 8]. Light microscopy evaluation of FS is
63 also prone to a certain degree of subjectivity [9].

64

65 During the last decade, the field of digital pathology has evolved significantly. Whole-
66 slide imaging (i.e. slide digitization) is now feasible with magnification and spatial
67 image quality comparable to conventional light microscopy [10]. Digital pathology
68 using digitized microscopy samples, or whole slide images (WSI), has multiple
69 advantages, such as enabling remote access to samples for consultation purposes
70 and remote sample analysis, and thus reducing the need for on-site experts. Another
71 significant advantage is the possibility of utilizing digital image analysis to facilitate

72 sample analysis [11]. Studies suggest that the use of WSI to interpret FS samples at
73 a distance is feasible with results comparable to conventional methods [12], and this
74 technique is already being utilized in clinical settings at certain locations where on-
75 site access to a pathologist is limited [13]. Currently however, the digitization of FS
76 has to be carried out with high-end, whole slide scanners, which mainly due to their
77 high cost (retail prices ranging from 30 000 - 200 000 €) are limited to well-equipped
78 clinics. These devices also tend to be bulky in size and require trained personnel and
79 regular maintenance, further limiting their usability for point-of-care slide scanning
80 [14].

81

82 During recent years, studies have demonstrated how extremely cost-efficient digital
83 microscopy devices for point-of-care microscopy diagnostics can be constructed
84 using commonly available, low-cost, mass-produced components from consumer
85 electronic products (typically smart phone camera systems) [15]. As the performance
86 of smart phone cameras has improved significantly during the last decade, the
87 imaging performance of this type of devices has also increased accordingly. Studies
88 suggest that the image quality achievable with this type of devices and components
89 is sufficient for diagnostic purposes in a variety of diseases, such as parasitic
90 diseases [16, 17], routine cancer histopathology [18]. Currently these devices have
91 certain limitations, one being that the digitized area typically is limited to a single
92 field-of-view (FOV) of the device.

93

94 Here, we studied the performance of a prototype, low-cost, mobile digital microscope
95 scanner which supports digitization of sample areas measuring multiple FOVs, i.e.
96 whole slide imaging. We evaluate the performance of the device for digitization of

97 routinely prepared, intraoperative breast cancer frozen sections. The WSIs captured
98 with the miniature microscope prototype are assessed by two independent
99 pathologists to detect metastases and results compared to conventional microscopy
100 and to analysis of WSIs captured with a high-end scanner.

101

102 **Materials and methods**

103 **Sample collection**

104 Samples used in this study were routinely collected sentinel lymph node frozen
105 sections, acquired during breast cancer surgery at hospitals within the Hospital
106 District of Helsinki and Uusimaa in southern Finland. The samples were collected
107 and prepared in accordance with local standard operating procedures during a
108 period of one year (2016), and archived in the files of the pathology laboratory of the
109 hospital district (HUSLAB, Helsinki, Finland). Frozen sections were cut with a
110 thickness of 5 μm , and routine staining performed using toluidine blue and anti-
111 cytokeratin immunohistochemical staining. Immunostaining for cytokeratins was
112 performed with a staining kit containing mouse monoclonal antibodies, targeting a
113 variety of cytokeratins, and diaminobenzidine as a chromogen (Cytone1 Plus kit,
114 Jilab Inc., Tampere, Finland).

115

116 For this study, we retrospectively identified and collected samples from a total
117 number of 80 patients. Of these, 28 patients were node positive (i.e. histologically
118 verified macro- or micrometastases) and 52 patients were node negative (i.e. no
119 detected cancer cells). A majority of patients had sections stained with both toluidine
120 blue and anti-cytokeratin antibodies, but for a minority of selected patients only

121 toluidine blue sections (n = 3) or anti-cytokeratin stained sections (n = 3) were
122 available. For this study, we decided to limit the analysis to one area of
123 representative tissue from every glass slide, selected visually by light microscopy
124 expert evaluation. For every patient, one representative glass slide stained with
125 toluidine blue and the corresponding slide, stained with anti-cytokeratin (if available)
126 was collected after which representative sample regions, measuring approximately
127 0.5 x 0.5 cm (25 mm²), were selected and marked by a pathologist (SN) for
128 digitization and further analysis.

129

130 The ground truth in the study was decided as the light microscopy diagnosis of the
131 physical frozen sections, performed by a pathologist experienced in breast cancer
132 pathology. Thus, after the slides had been collected, all slides were examined by a
133 pathologist (SN) to confirm diagnosis used as the study ground truth. One sample
134 was excluded during this phase, as staining artefacts affected sample quality.

135

136 **Digitization of samples**

137 The evaluated instrument is a portable, lightweight, cloud-connected digital
138 microscope scanner prototype developed by the Institute for Molecular Medicine
139 Finland – FIMM, University of Helsinki (Fig 1). The imaging optics of the microscope
140 is constructed using low-cost, mass produced polymer lenses, primarily developed
141 for usage in cell phone camera systems. The prototype was manufactured by a
142 company specialized in providing services for the microelectronics industry (Laser
143 Probe LP Oy, Oulu, Finland). Total material costs for the miniaturized imaging optics
144 in the device, including the integrated focusing system, are comparable to costs of
145 the optics of a mid-range smartphone. A white light-emitting diode (LED) is used as

146 the source of light for brightfield imaging, and by utilizing a retractable ultraviolet LED
147 source with adjacent filters, transmitted light fluorescence imaging is also supported.
148 The camera module (See3CAM_130, e-con Systems Inc., St Louis, USA) of the
149 microscope features a 13-megapixel complementary metal oxide semiconductor
150 (CMOS) sensor with a plastic 1/3.2" lens and a maximum image resolution of 4208 x
151 3120 pixels. The field of view of the microscope is approximately 0.93 x 0.69 mm²
152 with a pixel size of approximately 0.22 μm x 0.22 μm and the spatial resolution 0.9
153 μm, as measured using a standardized USAF resolution test chart (Fig 2). Coarse
154 focus is adjusted manually using a physical focus lever to adjust focus plane, and
155 fine focus automatically using the built-in auto focus-routine. The device is
156 connected, powered and operated through a universal serial bus (USB) connector
157 from a computer running a custom software written in the matrix laboratory
158 programming environment (MATLAB, MathWorks Inc, Natick, MA) to control the
159 device. The software features a live-view of the sample area, and controls to select
160 and adjust areas to be scanned. Adjustment of the glass slide can be performed
161 manually, or by utilizing the external motor unit to adjust sample position. Digitization
162 of larger sample areas (i.e. whole slide scanning), covering multiple field of views, is
163 possible by utilizing the external motor unit for automatic sample navigation while the
164 device automatically captures a series of images from the different location. Acquired
165 images are saved locally on the computer and uploaded to an image processing and
166 management platform (WebMicroscope, Fimmic Oy, Helsinki, Finland) running on a
167 cloud server located at the university campus (Meilahti Campus Library Terkko,
168 University of Helsinki, Helsinki, Finland). Scanned areas measuring multiple FOVs
169 are stitched together after the scanning process into a single virtual slide. We used
170 the commercially available software Image Composite Editor (Microsoft

171 Computational Photography Research Group, Microsoft Inc., Redmond, WA) for the
172 image stitching process. The generated digital samples were saved in the Tagged
173 Image File Format (TIFF), and further compressed to a wavelet file format
174 (Enhanced Compressed Wavelet; ECW, Hexagon Geospatial, Wisconsin, USA)
175 with a target compression ratio of 1:9 to reduce file size, before uploading to the
176 image management platform. As shown in earlier work, this amount of compression
177 preserves sufficient spatial detail to not alter results significantly [19] . Remote
178 access to the image server for sample viewing and scoring was established using a
179 web browser, secured with SSL encryption.

180

181 **Fig 1. Miniature microscope scanner prototype.** Left: Miniature microscope
182 scanner “MoMic” (red bounding box) next to reference whole slide scanner. Right:
183 Overview of the device showing main microscope unit housing camera module (A),
184 motor unit for sample navigation (B) and glass slide holder (C).

185

186 **Fig 2. US Air Force 1951 three-bar resolution test chart.** Images captured with
187 miniature microscope scanner. Enlarged images showing smallest resolvable bars
188 (group 9, element 2 - 3), corresponding to a spatial resolution of approximately 0.9
189 μm .

190

191 The samples used in this study were also digitized using a high-end, automated
192 whole slide scanner (Pannoramic P250, 3DHistech Ltd., Budapest, Hungary). The
193 slide scanner uses a 20x objective (NA 0.8) equipped with a three-CCD (charge-
194 coupled device) digital camera with a pixel resolution of 0.22 μm . The acquired
195 images were compressed with a compression ratio of 1:9 to a wavelet file format and

196 uploaded to the whole-slide management server, using the configurations described
197 above.

198

199 **Slide management and remote analysis of virtual slides**

200 We used the image management platform described above to upload the virtual
201 slides into slide collections for evaluation by the pathologists. Based on these
202 collections of virtual slides, two separate online scoring questionnaires were created
203 for sample evaluations (one for each device) (Fig 3). The scoring system displayed
204 one patient case at a time, starting with the toluidine blue stained sample, after which
205 corresponding anti-cytokeratin stained section was displayed. If only one type of
206 staining was available, only this slide was displayed before continuing to the next
207 case. Display order of patient cases was randomized for both experts, and also for
208 the virtual samples from the separate devices. For every displayed virtual slide, the
209 pathologist was presented with three possible diagnostic categories: “Metastasis”,
210 “No metastasis” and “Not evaluable”. An option for inputting additional comments
211 was also provided for each sample, and experts were encouraged to comment on
212 slide quality during the scoring process. Two independent pathologists evaluated the
213 samples using the online scoring system, which was accessible through a link, sent
214 by e-mail.

215

216 **Figure 3. Online image management platform and slide scoring questionnaire.**

217 Image showing a scanned lymph node frozen sections (digitized with the miniature
218 microscope scanner) and viewed on the slide management platform with the scoring
219 questionnaire.

220

221

222 **Statistical analysis**

223 Analysis of results and statistical calculations were performed using a general-
224 purpose statistical software package (Stata 15.1 for Mac, Stata Corp., College
225 Station, TX, USA). For statistical analysis, individual samples were classified as
226 either positive for metastatic tissue (i.e. presence of either macro- or
227 micrometastases) or negative for metastatic tissue (i.e. no visible cancer cells).
228 Samples not evaluable according to the pathologists were excluded. Concordance
229 between the miniature microscope scanner, the reference slide scanner and the
230 ground truth was estimated with kappa statistics (kappa values 0.01–0.20 were
231 considered as slight, 0.21–0.40 fair, 0.41–0.60 moderate, 0.61–0.80 good and 0.81–
232 1.00 as high agreement) [20]. Sensitivity for detection of metastatic cells was
233 calculated as the percentage of true positives (TP) divided by TP and false negatives
234 (FN), with conventional light microscopy analysis as the ground truth (GT).
235 Specificity was calculated as the percentage of true negatives (TN) divided by TN
236 and false positives (FP).

237

238 **Results**

239 The total number of slides analyzed after exclusion of samples not evaluable by the
240 pathologists was 152, from 79 patients. By light microscopy 27 (34 %) of these
241 patients were node positive, with 24 (30 %) having macrometastases and 3 (4 %)
242 micrometastases. Correspondingly, 52 patients (66 %) were node negative. When
243 comparing analysis of whole slide images (WSIs) scanned with the miniature
244 microscope scanner to the ground truth, mean overall sensitivity for detection of

245 metastases was 90.56 % (93.88 % and 87.23 %), and mean specificity 99.03 %
 246 (100.00% and 98.06 %), on a slide level. When comparing analysis of WSIs from the
 247 reference slide scanner to the ground truth, a mean sensitivity of 93.80 % (95.92 %
 248 and 91.67 %) for detection of metastases was observed and a mean specificity of
 249 99.03 % (98.06 % and 100.00 %) (Table 1).

250

251 **Table 1. Accuracy for detection of metastases by pathologist analysis of virtual**
 252 **slides, scanned with both microscope scanners.**

Device	Sensitivity (%)	Specificity (%)	False Negative	False Positive	Not Evaluable
MoMic (Expert 1)	93.88	100	3	0	2
MoMic (Expert 2)	87.23	98.06	6	2	2
Reference Scanner (Expert 1)	95.92	98.06	2	1	1
Reference Scanner (Expert 2)	91.67	100.00	4	0	3

253 Table showing overall sensitivity, specificity, total number of FN and FP, and slides
 254 classified as not evaluable. Results calculated on a slide level, compared to ground
 255 truth.

256

257 When measuring agreement between experts, a strong concordance between
 258 results from the miniature microscope scanner and ground truth was observed for
 259 both experts ($k = 0.95$ and $k = 0.87$). Results from the analysis of reference scanner
 260 WSIs also showed a strong concordance with the ground truth for both experts ($k =$
 261 0.95 and $k = 0.94$). Furthermore, strong intraobserver agreement for both
 262 pathologists was observed when comparing results from both scanners for the same
 263 expert ($k = 0.94$ and $k = 0.92$) (Table 2).

264

265 **Table 2. Agreement of results for detection of metastases in slides scanned**
 266 **with the miniature microscope scanner and the reference slide scanner.**

Device	Ground Truth	Momic (Expert 1)	Reference scanner (Expert 1)	Momic (Expert 2)	Reference scanner (Expert 2)
Ground Truth	1				
Momic (Expert 1)	$k = 0.95$ (CI95%: 0.90 - 1.00)	1			
Reference scanner (Expert 1)	$k = 0.95$, (CI95%: 0.90 - 1.00)	$k = 0.94$ (CI95%: 0.88 - 1.00)	1		
Momic	$k = 0.87$, (CI95%: 0.79 -	$k = 0.92$ (CI95%: 0.84 -	$k = 0.86$ (CI95%: 0.77 -	1	

(Expert 2)	0.96)	0.99)	0.95)		
Reference scanner (Expert 2)	k = 0.94, (CI95%: 0.88 - 1.00)	k = 0.95 (CI95%: 0.90 - 1.00)	k = 0.92 (CI95%: 0.85 - 0.99)	k = 0.92 (CI95%: 0.85 - 0.99)	1

267 Comparison of analysis of slides. Agreement calculated using kappa statistics with
 268 associated confidence intervals (95%); $p < 0.001$ for all values shown.

269

270 The number of false negatives (FN) in the analysis of WSIs scanned with the
 271 miniature microscope scanner was 3 (2 %) and 6 (4 %), for the experts. Two
 272 samples (1 %) were incorrectly classified as tumor positive by one expert with the
 273 miniature microscope scanner, and no false positives (FP) were detected by the
 274 other expert. The number of FN slides in the analysis of WSIs from the reference
 275 slide scanner was 2 (1 %) and 4 (3 %). For the WSIs from this device, a single FP (1
 276 %) was detected by the first expert, and none by the second. Two slides (1 %) were
 277 classified as not evaluable by both experts when analyzing slides from the miniature
 278 microscope scanner (different slides for both experts). The number of reference
 279 scanner WSIs classified as not evaluable was 1 (1 %) and 3 (2 %).

280

281 On a patient level, i.e. including available slides with both staining methods for each
 282 patient, the pathologists classified the WSIs from two patients (3 %) incorrectly as
 283 tumor negative with the miniature microscope scanner. For the slides scanned with
 284 the reference slide scanner, one patient (1 %) was incorrectly classified as tumor
 285 negative. This case was the same patient, classified incorrectly as tumor negative in
 286 the WSIs from the miniature microscope scanner (Table 3). There were no FP on a

287 patient level with either device. For one patient, both available slides (1 %) were
 288 classified as not evaluable by one expert with the miniature microscope scanner.
 289
 290 **Table 3. Patient cases diagnosed incorrectly in analysis of WSIs from both**
 291 **scanners, compared to light microscopy.**

Case number	Staining type of sample	Light microscopy diagnosis (Ground truth)	MoMic WSI (Expert 1)	Reference slide scanner WSI (Expert 1)	MoMic WSI (Expert 2)	Reference slide scanner WSI (Expert 2)
1	Toluidine blue	Micrometastasis	No metastasis (FN)	Metastasis	No metastasis (FN)	No metastasis
	IHC	Micrometastasis	No metastasis (FN)	Metastasis	Metastasis	Metastasis
2	Toluidine blue	Micrometastasis	No metastasis (FN)	No metastasis (FN)	No metastasis (FN)	No metastasis (FN)
	IHC	Not available	Not available	Not available	Not available	Not available
3	Toluidine blue	Macrometastasis	Metastasis	Metastasis	No metastasis (FN)	Metastasis

	IHC	Macrometastasis	Metastasis	Metastasis	No metastasis (FN)	Metastasis
4	Toluidine blue	No metastasis	Not evaluable	No metastasis	No metastasis	No metastasis
	IHC	No metastasis	Not evaluable	No metastasis	No metastasis	No metastasis

292 Table showing discrepant patient cases, compared to light microscopy. Included also
 293 one case with both miniature microscope scanner WSIs classified as not evaluable
 294 by one expert (number 4).

295

296 Discussion

297 In this article we evaluate a prototype of a portable, miniature digital microscope
 298 scanner for diagnostic assessment of lymph node frozen sections, obtained during
 299 breast cancer surgery. Key features of the device include support for whole slide
 300 scanning, cloud-connectivity and the use of significantly more inexpensive
 301 components, compared to conventional devices. We used the device to digitize
 302 archived sentinel lymph node frozen sections and two pathologists with experience
 303 in breast cancer histopathology assessed the whole slide images for the detection of
 304 metastases. Results were compared to analysis of the same samples scanned with
 305 a high-end slide microscope scanner and to pathologist light microscopy analysis of
 306 the slides.

307

308 Overall, we observed a strong concordance in results from both devices for detection
 309 of metastases, compared to light microscopy as study ground truth (GT). A slightly

310 higher concordance to the GT was observed in results from the reference slide
311 scanner (mean $k = 0.95$), than in results from the miniature microscope scanner
312 (mean $k = 0.91$). Agreement between the pathologists was strong ($k = 0.92 - 0.94$).

313

314 Overall sensitivity and specificity for detection of metastases was high for both the
315 miniature microscope scanner (sensitivity 90.56 % and specificity 99.03 %) and the
316 reference slide scanner (sensitivity 93.80 % and specificity 99.03%). Overall, the rate
317 of false negatives (FN) and false positives (FP) was low for both devices, although
318 FN rate was marginally higher with the miniature microscope scanner, and few whole
319 slide images (WSIs) were classified as not evaluable. These results suggest that
320 analysis of slides scanned with both devices yield comparable results, with an overall
321 high grade of sensitivity and specificity.

322

323 When grouping available slides from the same patient together, few major
324 discrepancies was observed on a patient level. The slides for two patients were
325 classified incorrectly as negative with the miniature microscope scanner. One of
326 these cases was the same for both experts and also classified incorrectly as
327 negative with the reference slide scanner. This patient had micrometastases, but
328 only toluidine blue-stained sections available, representing a challenging sample (Fig
329 4). The second patient diagnosed incorrectly as negative by one expert with the
330 miniature microscope scanner also had micrometastases (Fig 5), but both staining
331 methods available. These slides were correctly diagnosed by the second expert. The
332 final discrepant patient case with the miniature microscope scanner, classified
333 incorrectly as negative by one expert, represented a sample with a macrometastasis
334 covering almost the entire section (Fig 6). This sample had sections with both

335 staining methods available, and slides for this case were correctly diagnosed by the
336 second expert. On a patient level, we observed no FP with either device.

337

338 **Figure 4. Toluidine blue stained frozen sections with micrometastasis.** Slide
339 scanned with the miniature microscope scanner (upper images), and reference slide
340 scanner (lower images). Anti-cytokeratin staining was not available for this section,
341 making analysis challenging, and sample was incorrectly classified as negative by
342 both experts, regardless of device used for digitization.

343

344 **Figure 5. Anti-cytokeratin stained frozen section with micrometastasis.** Slide
345 scanned with miniature microscope scanner (left), and reference slide scanner
346 (right). Red bounding box showing higher magnification (a. miniature scanner, and b.
347 reference slide scanner).

348

349 **Figure 6. Lymph node frozen section with macrometastasis, stained with both**
350 **anti-cytokeratin (upper row) and toluidine blue (lower row) staining.** Overview of
351 area scanned with miniature microscope (left), red bounding box (A. and B.) showing
352 enlarged area (a. and b.). Reference scanner corresponding regions for comparison
353 purposes shown to the right (C. and c.).

354

355 On a slide level, a majority of incorrectly classified WSIs from both devices were
356 toluidine blue slides, and slides with micrometastases. A majority of toluidine blue
357 sections were correctly diagnosed in consecutive anti-cytokeratin stained slides.
358 Detection of metastases in toluidine blue staining is known to be less reliable,
359 especially for smaller lesions [21]. Furthermore, micrometastases in regional lymph

360 nodes are associated with a reduced overall survival, but the exact clinical
361 significance is being debated [22]. Only one major discrepancy was observed on a
362 patient level, where a macrometastasis was misdiagnosed with the miniature
363 microscope scanner WSIs by one expert, suggesting an overall high sensitivity for
364 detection of macrometastases in slides from this device. Among the results from the
365 same expert, a significant part of FN (20 - 30 %) were incorrectly classified in WSIs
366 from both scanners, suggesting other causes for discrepancy than only difference in
367 image quality.

368

369 Both pathologists were asked to comment on the quality of virtual slides. A majority
370 of the feedback concerned technical problems, such as areas being out of focus (for
371 both devices), “vignetting” of certain samples (mainly the miniature microscope
372 images) and poor tissue sample quality (in physical slide) (S1 Fig). Most of these
373 problems were related to slide scanning, and could be solved by rescanning affected
374 slides. Interestingly, technical quality did not seem to correlate with accuracy of final
375 sample interpretation, as all samples with comments regarding quality were
376 nonetheless correctly interpreted. Additional comparison WSIs from both devices
377 can be found in the supplementary material (S2 Fig.).

378

379 As this is an early study, there is a number of limitations. Our patient material
380 included a relatively small number of micrometastases, and no cases of ITCs.
381 Furthermore, only a single area per slide was digitized. A potential source of bias in
382 this study is that one of the experts analyzing the WSIs (SN) had originally selected
383 the slide areas to be digitized. As WSIs were displayed in a randomized order during
384 analysis, and sample collection was performed in early stages of the study, we

385 believe the risk of significant bias is relatively small. In this study we have focused
386 mainly on image quality of virtual slides, but especially if larger amounts of slides are
387 scanned, additional factors needed to be considered in clinical applications include
388 e.g. turnover time for slide scanning and data connectivity for uploading of digitized
389 slides.

390

391 Results here suggest that by using a portable, miniature microscope scanner
392 constructed out of components that are several orders of magnitude cheaper
393 compared to components in currently available scanners, routine breast cancer
394 lymph node frozen sections can be scanned with sufficient quality for detection of
395 metastases. Our work here demonstrates how inexpensive, mass-produced
396 components can be utilized to develop novel solutions for point-of-care slide
397 digitization, and potentially improve access to digital diagnostics and facilitate
398 sample analysis. This technology could likely be expanded also for real time analysis
399 of samples at the point-of-care, e.g. for intraoperative applications. Recent studies
400 show promising results for detection of metastases using deep learning-based image
401 analysis in sentinel lymph node samples, scanned with high-end scanners (23)(24).
402 As our results here suggest that image quality achievable with low-cost components
403 can be comparable, this type of image analysis could likely be applied to samples
404 scanned using this technology also. Further research is needed to validate these
405 results and should focus on evaluating the technology in clinical environments.

406

407 **Conclusion**

408 Breast cancer lymph node metastases in frozen sections can be accurately detected
409 by visual analysis of digitized slides, scanned with a low-cost, point-of-care slide

410 scanner, with results comparable to conventional light microscopy and analysis of
411 slides scanned with a high-end whole slide scanner. This method could potentially
412 provide a novel platform for digital diagnostics, especially in resource-limited
413 settings, facilitate sample analysis and reduce the need for experts on-site during
414 surgical procedures.

415

416 **References**

417 (1) Siegel RL, Miller KD, Jemal A. Cancer statistics, 2018. *CA: a Cancer Journal for*
418 *Clinicians* 2018 Jan;68(1):7-30.

419 (2) Fisher B, Bauer M, Wickerham DL, Redmond CK, Fisher ER, Cruz AB, et al.
420 Relation of number of positive axillary nodes to the prognosis of patients with primary
421 breast cancer. An NSABP update. *Cancer* 1983 Nov 01;52(9):1551-1557.

422 (3) Mansel RE, Fallowfield L, Kissin M, Goyal A, Newcombe RG, Dixon JM, et al.
423 Randomized multicenter trial of sentinel node biopsy versus standard axillary
424 treatment in operable breast cancer: the ALMANAC Trial. *J Natl Cancer Inst* 2006
425 May 03;98(9):599-609.

426 (4) Samphao S, Eremin JM, El-Sheemy M, Eremin O. Management of the axilla in
427 women with breast cancer: current clinical practice and a new selective targeted
428 approach. *Annals of Surgical Oncology* 2008 May;15(5):1282-1296.

429 (5) Weiser MR, Montgomery LL, Susnik B, Tan LK, Borgen PI, Cody HS. Is routine
430 intraoperative frozen-section examination of sentinel lymph nodes in breast cancer
431 worthwhile?. *Annals of Surgical Oncology* 2000 Oct;7(9):651-655.

- 432 (6) Lucci A, McCall LM, Beitsch PD, Whitworth PW, Reintgen DS, Blumencranz PW,
433 et al. Surgical complications associated with sentinel lymph node dissection (SLND)
434 plus axillary lymph node dissection compared with SLND alone in the American
435 College of Surgeons Oncology Group Trial Z0011. *Journal of Clinical Oncology* 2007
436 Aug 20;25(24):3657-3663.
- 437 (7) Liu L, Lang JE, Lu Y, Roe D, Hwang SE, Ewing CA, et al. Intraoperative frozen
438 section analysis of sentinel lymph nodes in breast cancer patients. *Cancer*
439 2011;117(2):250-258.
- 440 (8) Holck S, Galatius H, Engel U, Wagner F, Hoffmann J. False-negative frozen
441 section of sentinel lymph node biopsy for breast cancer. *Breast* 2004 Feb;13(1):42-
442 48.
- 443 (9) Yeh Y, Nitadori J, Kadota K, Yoshizawa A, Rekhtman N, Moreira AL, et al. Using
444 frozen section to identify histological patterns in stage I lung adenocarcinoma of ≤ 3
445 cm: accuracy and interobserver agreement. *Histopathology* 2015 Jun;66(7):922-938.
- 446 (10) Weinstein RS, Descour MR, Liang C, Barker G, Scott KM, Richter L, et al. An
447 array microscope for ultrarapid virtual slide processing and telepathology. Design,
448 fabrication, and validation study. *Hum Pathol* 2004 Nov;35(11):1303-1314.
- 449 (11) Al-Janabi S, Huisman A, Van Diest PJ. Digital pathology: current status and
450 future perspectives. *Histopathology* 2012 Jul;61(1):1-9.
- 451 (12) Gifford AJ, Colebatch AJ, Litkouhi S, Hersch F, Warzecha W, Snook K, et al.
452 Remote frozen section examination of breast sentinel lymph nodes by telepathology.
453 *ANZ J Surg* 2012 Nov;82(11):803-808.

- 454 (13) Thorstenson S, Molin J, Lundström C. Implementation of large-scale routine
455 diagnostics using whole slide imaging in Sweden: Digital pathology experiences
456 2006-2013. *Journal of Pathology Informatics* 2014;5(1):14.
- 457 (14) Isaacs M, Lennerz JK, Yates S, Clermont W, Rossi J, Pfeifer JD.
458 Implementation of whole slide imaging in surgical pathology: A value added
459 approach. *Journal of Pathology Informatics* 2011;2:39.
- 460 (15) Zhu H, Isikman SO, Mudanyali O, Greenbaum A, Ozcan A. Optical imaging
461 techniques for point-of-care diagnostics. *Lab on a Chip* 2013 Jan 07;13(1):51-67.
- 462 (16) Holmström O, Linder N, Ngasala B, Mårtensson A, Linder E, Lundin M, et al.
463 Point-of-care mobile digital microscopy and deep learning for the detection of soil-
464 transmitted helminths and *Schistosoma haematobium*. *Glob Health Action* 2017
465 Jun;10(sup3):1337325.
- 466 (17) Pirnstill CW, Cote GL. Malaria Diagnosis Using a Mobile Phone Polarized
467 Microscope. *Scientific Reports* 2015 Aug 25;5:13368.
- 468 (18) Holmström O, Linder N, Lundin M, Moilanen H, Suutala A, Turkki R, et al.
469 Quantification of Estrogen Receptor-Alpha Expression in Human Breast Carcinomas
470 With a Miniaturized, Low-Cost Digital Microscope: A Comparison with a High-End
471 Whole Slide-Scanner. *PLoS ONE [Electronic Resource]* 2015;10(12):e0144688.
- 472 (19) Konsti J, Lundin M, Linder N, Haglund C, Blomqvist C, Nevanlinna H, et al.
473 Effect of image compression and scaling on automated scoring of
474 immunohistochemical stainings and segmentation of tumor epithelium. *Diagnostic
475 Pathology* 2012;7:29.

- 476 (20) Landis JR, Koch GG. The measurement of observer agreement for categorical
477 data. *Biometrics* 1977 Mar;33(1):159-174.
- 478 (21) Chao C. The use of frozen section and immunohistochemistry for sentinel lymph
479 node biopsy in breast cancer. *Am Surg* 2004 May;70(5):414-419.
- 480 (22) Andersson Y, Bergkvist L, Frisell J, de Boniface J. Long-term breast cancer
481 survival in relation to the metastatic tumor burden in axillary lymph nodes. *Breast
482 Cancer Research & Treatment* 2018 Sep;171(2):359-369.
- 483 (23) Ehteshami Bejnordi B, Veta M, Johannes van Diest P, van Ginneken B,
484 Karssemeijer N, Litjens G, et al. Diagnostic Assessment of Deep Learning
485 Algorithms for Detection of Lymph Node Metastases in Women With Breast Cancer.
486 *JAMA* 2017;318(22):2199-2210.
- 487 (24) Liu Y, Kohlberger T, Norouzi M, Dahl GE, Smith JL, Mohtashamian A, et al.
488 Artificial Intelligence–Based Breast Cancer Nodal Metastasis Detection. *Arch Pathol
489 Lab Med* 2018.

490

491 **Supporting information**

492 **S1 Fig. Technical problems encountered in sample digitization.** A minority of
493 slides scanned with the miniature microscope scanner displayed a “vignetting” effect,
494 showing uneven color intensity in scanned images (left panel). This was likely
495 caused by problems with the brightfield correction algorithm. Areas in some WSIs
496 were out of focus (right panel), due to focusing problems. This affected small areas
497 in a minority of samples, scanned with both devices. Problems here were temporary,
498 and could be corrected by rescanning affected slides.

499 **S2 Fig. Lymph node frozen section with macrometastasis, stained with**
500 **toluidine blue (left) and anti-cytokeratin (right) staining, and scanned with both**
501 **devices.** Upper images showing overview of the FS section and lower side showing
502 enlarged areas (as indicated with red bounding boxes). Slides scanned with the
503 miniature microscope scanner on left side (A. and C.), and reference slide scanner
504 WSIs on the right side for comparison (B. and D.).

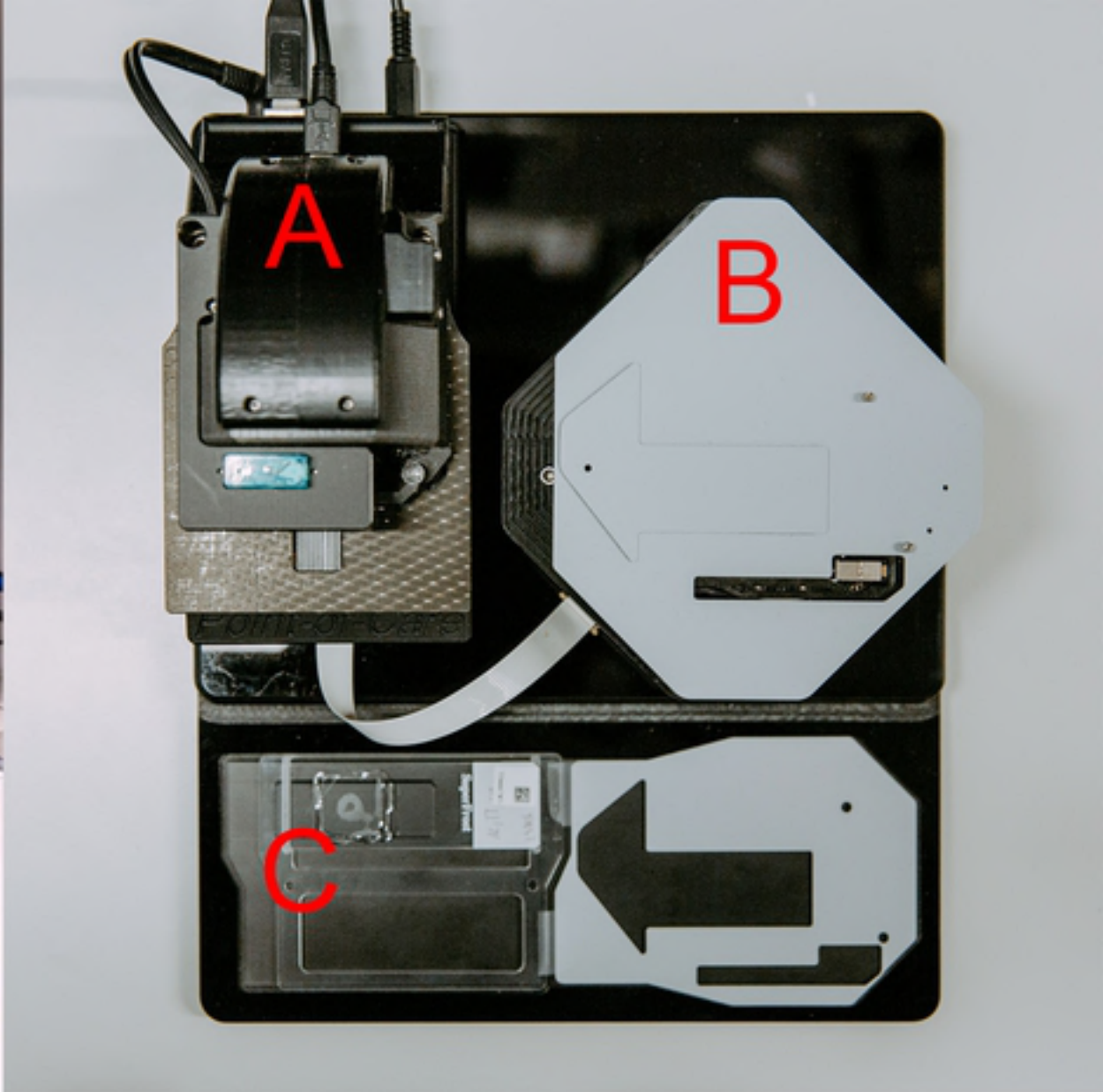


Figure 1

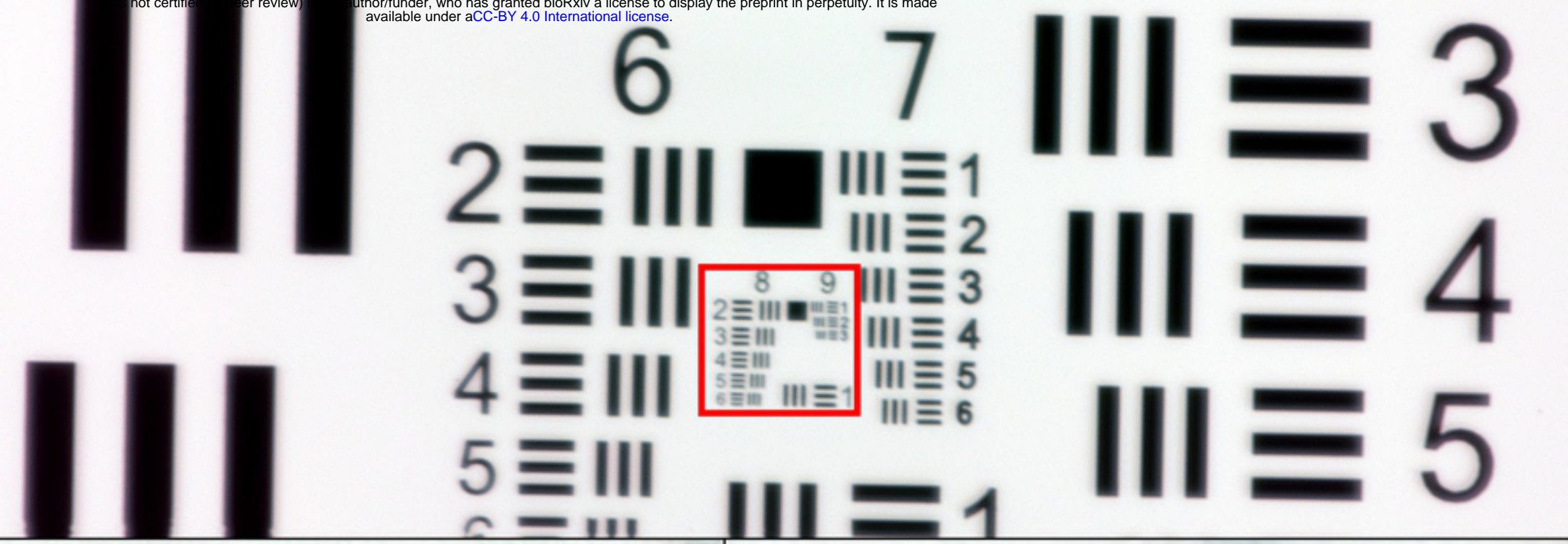
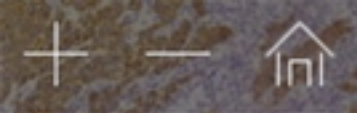
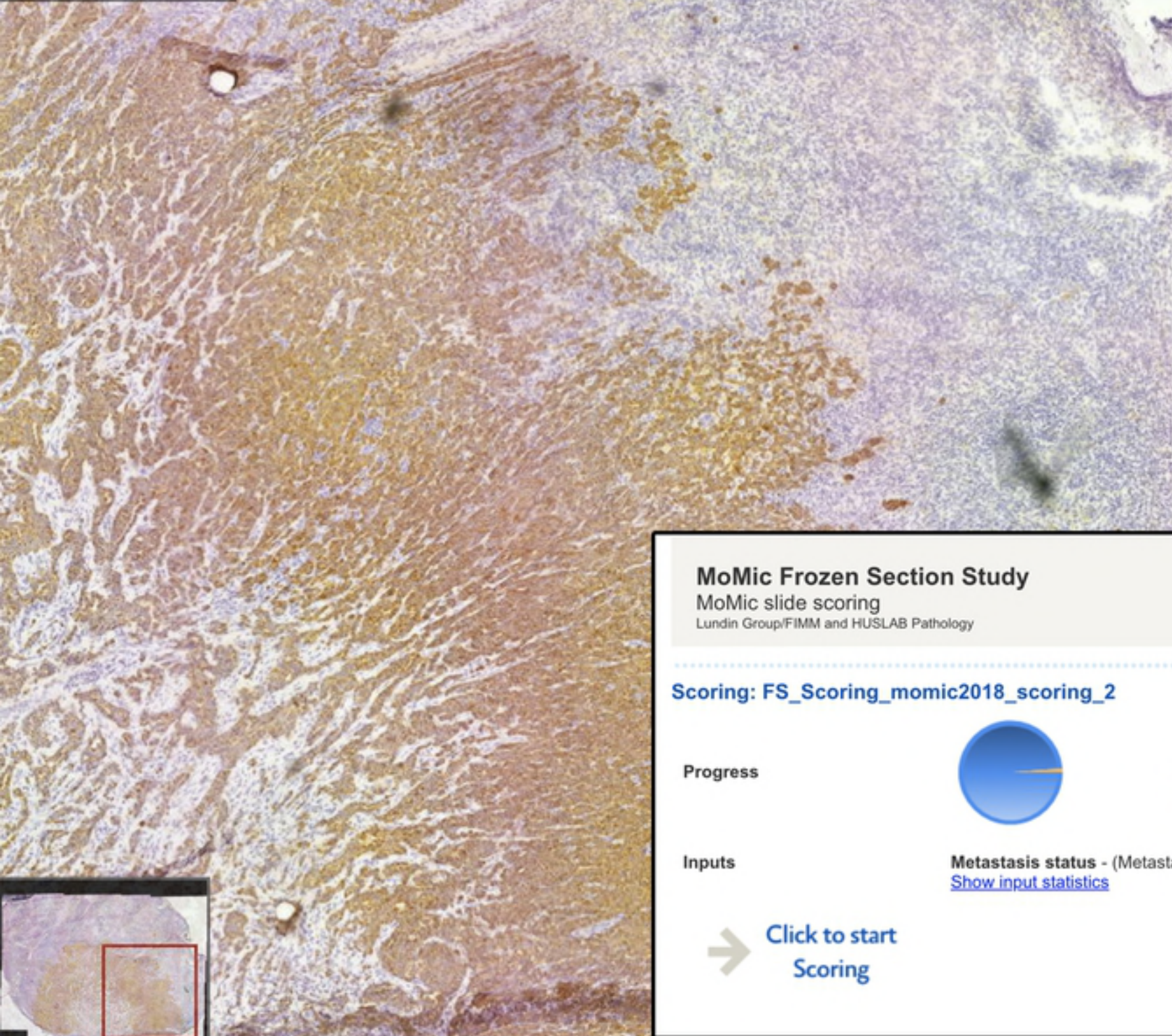


Figure 2



x2	x5	x10
x20	x40	x100



Metastasis status

Metastasis
 No metastasis
 Not evaluable

Add notes here


Submit



⊖ Current area (17/159) ⊕

First unscored First incomplete

MoMic Frozen Section Study
MoMic slide scoring
Lundin Group/FIMM and HUSLAB Pathology

Scoring: FS_Scoring_momic2018_scoring_2

Progress  **Nr of areas to score: 159**

	Scored (157)
	Unscored (2)

Inputs **Metastasis status** - (Metastasis, No metastasis, Not evaluable)
[Show input statistics](#)

➔ **Click to start Scoring**

Figure 3

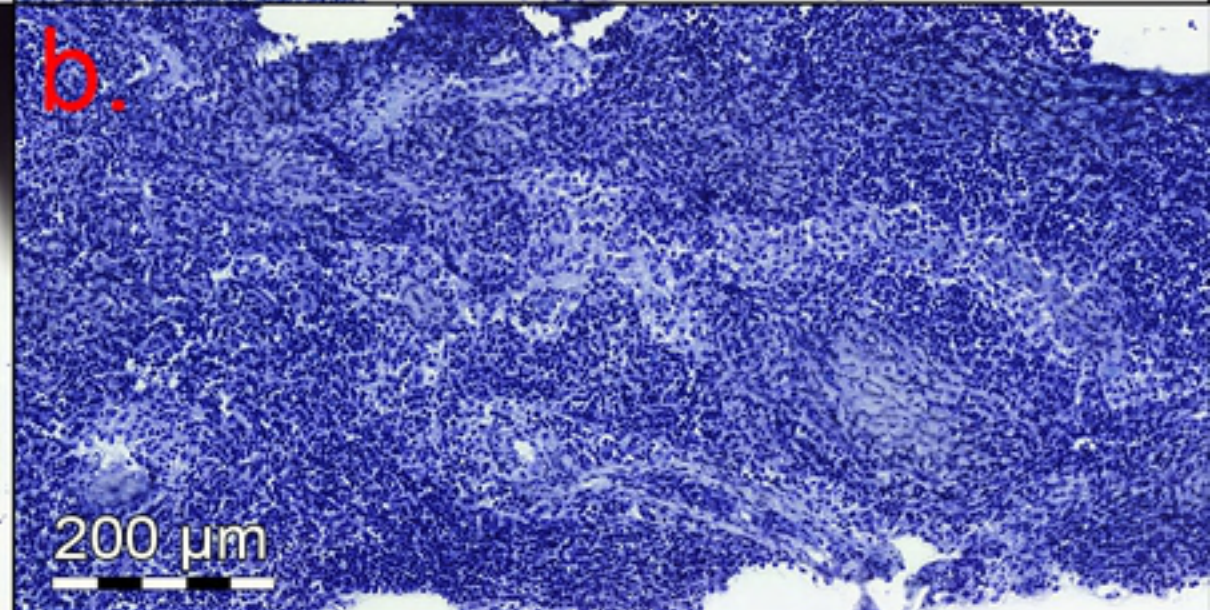
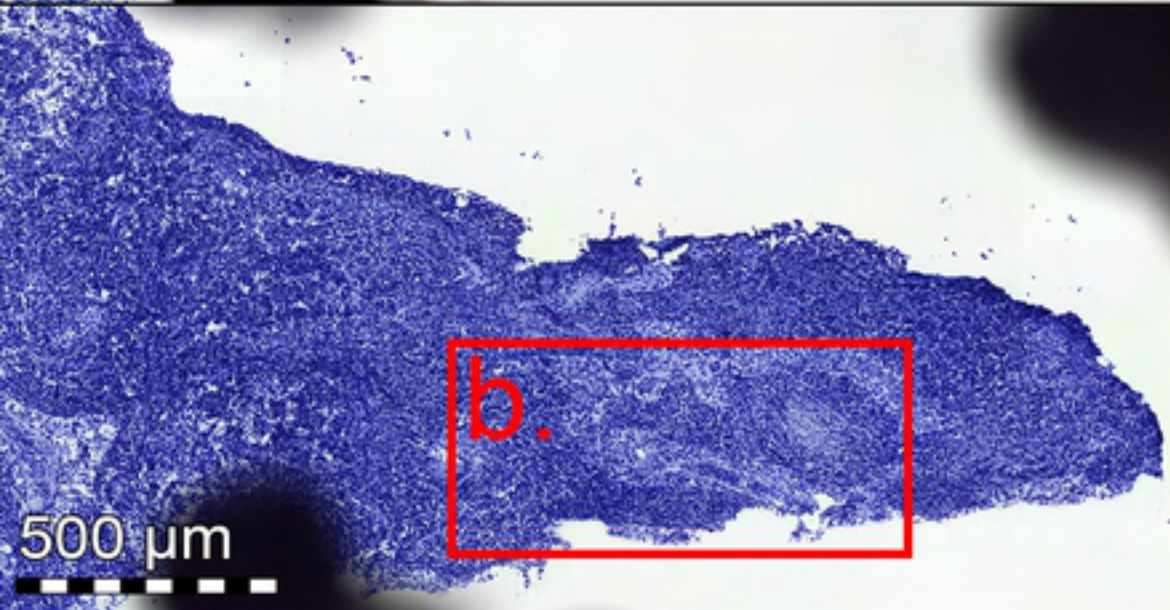
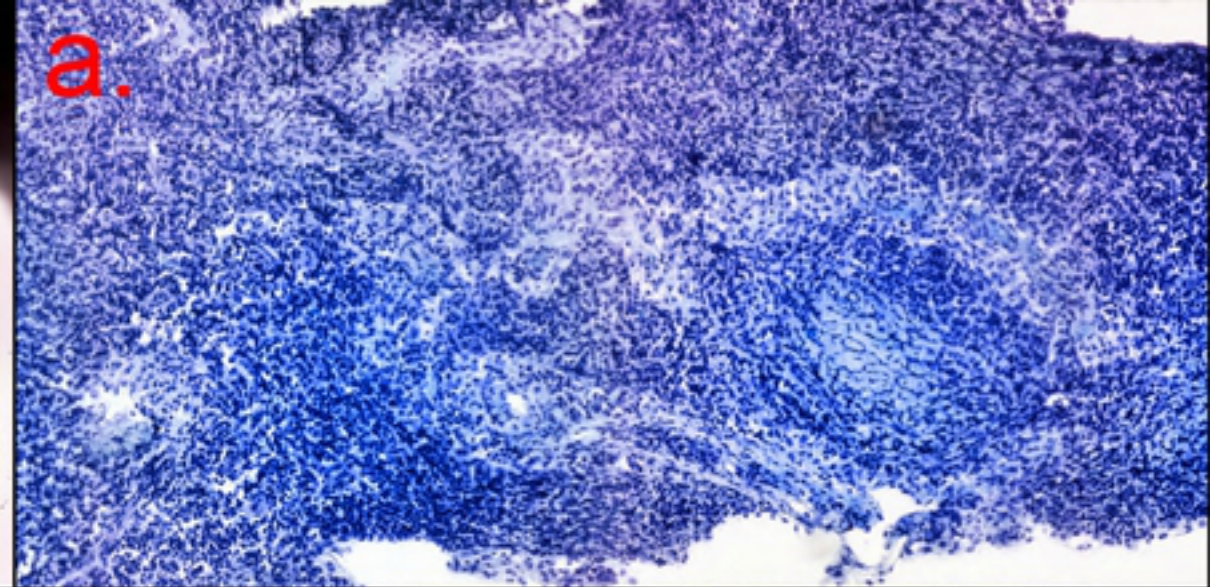
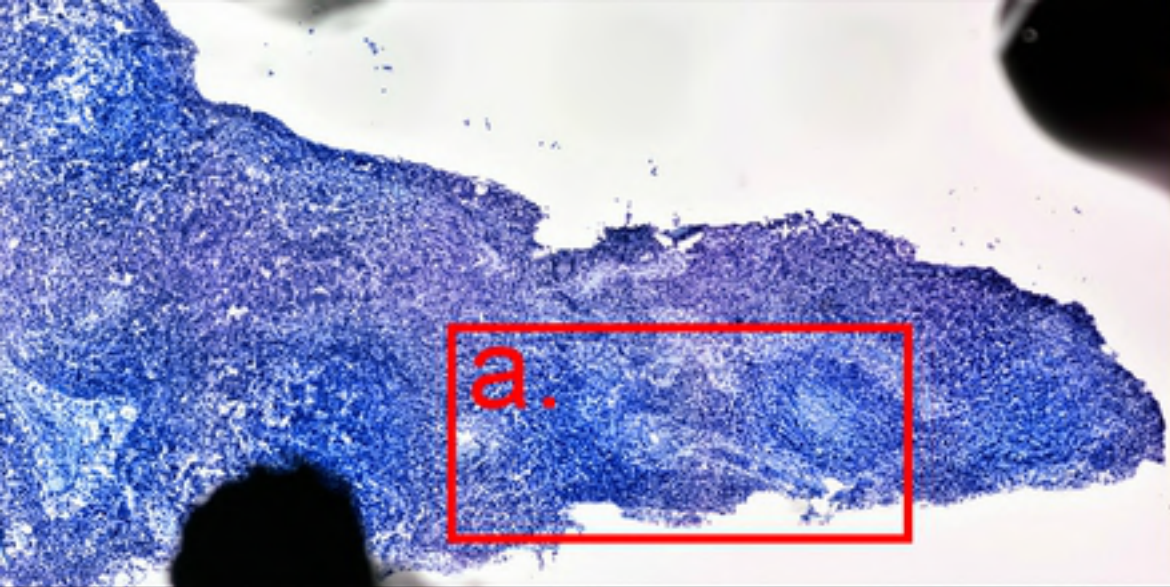


Figure 4

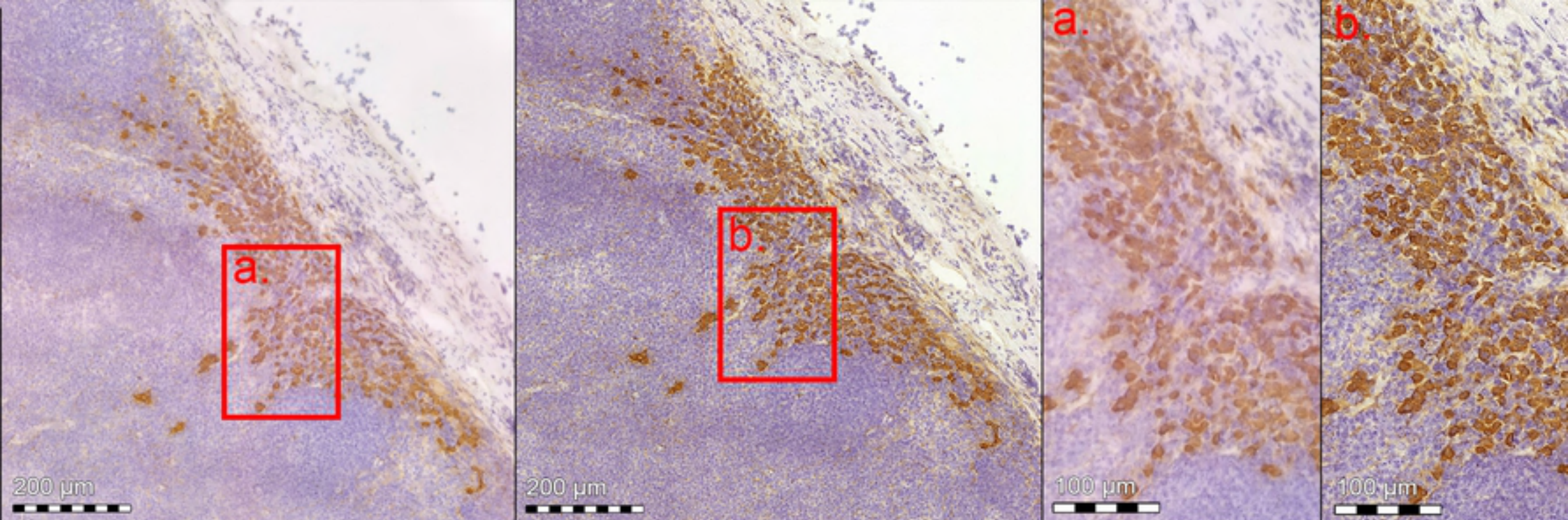


Figure 5

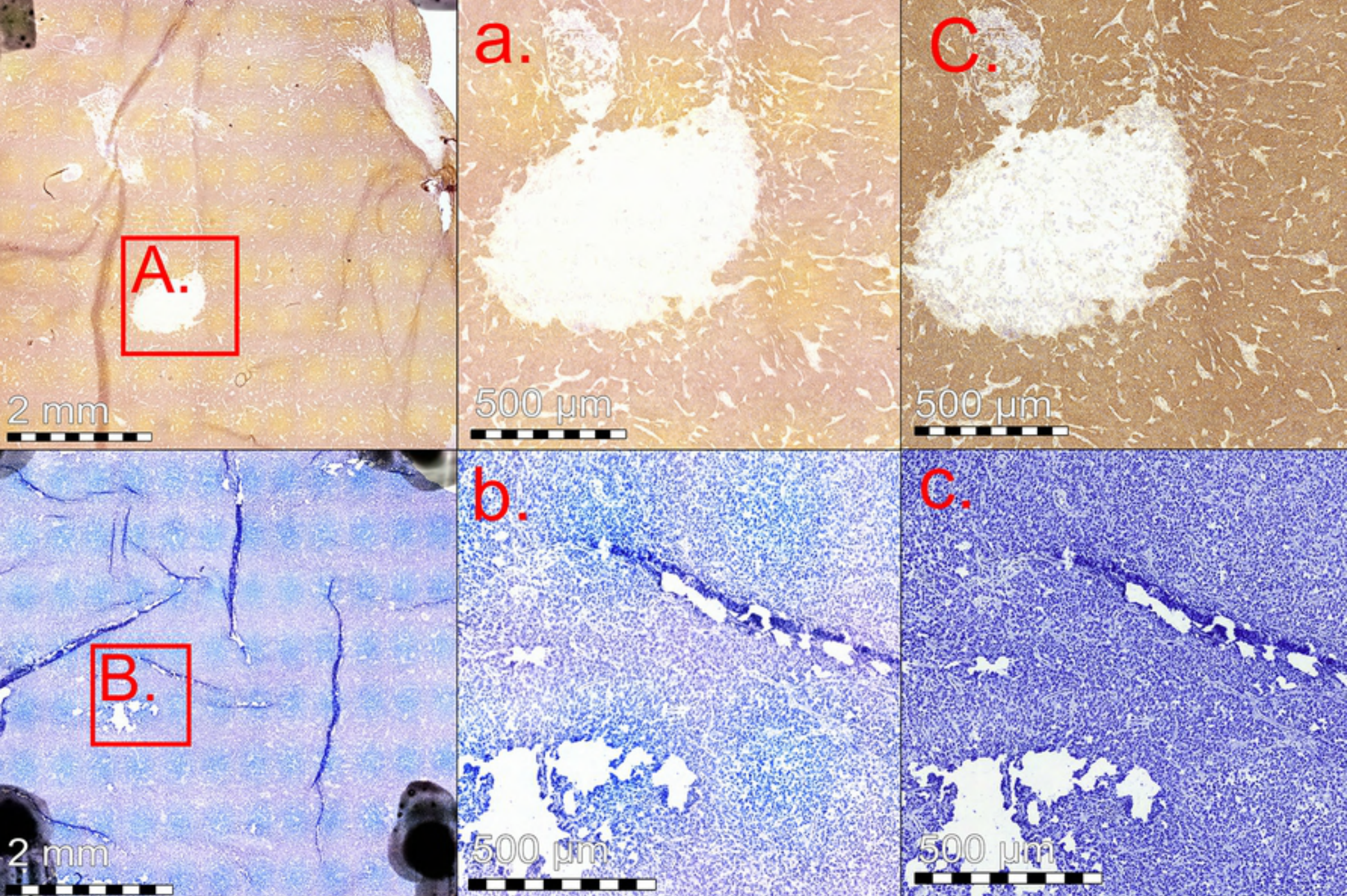


Figure 6